JFMSE, 32(1), pp. 49~64, 2020.
수산해양교육연구, 제32권 제1호, 통권103호, 2020.
www.ksfme.or.kr
https://doi.org/10.13000/JFMSE.2020.2.32.1.49

A Study on Speed Control Method of Propulsion Motor for Small Ships with AFE Converter

Jae-Jung HUR†
Korea Institute of Maritime and Fisheries(professor)

AFE 컨버터가 적용된 소형선박의 추진전동기 속도제어 방식에 관한 연구

허 재 정†
한국해양수산연수원(교수)

Abstract

Research of electric propulsion system have been conducted to minimize the occurrence of marine environmental pollution and maintenance costs in small ships such as coastal passenger ships, cruise ships and fishing boats. Speed control methods induction motor that are widely used in large electric propulsion ships has low control characteristics in the low speed range, and therefore, the performance of the steering is very deteriorated in ships with a large number of the entry and departure of port. Therefore, in this paper, the vector control algorithm with the AFE rectifier is applied to induction motor and speed control performance at low speed range has been improved. and it was verified through computer simulation using PISM program.

Key words : Induction motor, Direct torque control, Vector control, Electric propulsion ship, Control method

Ⅰ. Introduction

More generally for small ships such as coastal passenger ships, cruise ships, and small fishing boat, there have been on-going project or researches on methods to drive the electric propulsion motors by the electricity generated from eco-friendly renewable energy such as natural gas, fuel cells, solar energy, wind energy, etc. to minimize the occurrence of marine pollution and ship maintenance costs(Kim et al., 2009; Kim et al., 2008; Kim et al., 2012; Jeon et al., 2018; Kim et al.,2013).

Focus on the different types of motors used in maritime industry, they can be broadly classified into DC motors, AC motors and other motors, and AC motors can be divided into induction and synchronous motors. DC motor has been widely used in variable speed driving device because of simple control of flux amplitude and torque and excellent transient response. But, since there is a brush and commutator, it is necessary to repair and inspect it regularly. Due to the commutation limit of the commutator, there are some problems to

† Corresponding author: 051-620-5789, jjheo@seaman.or.kr/orcid.org/0000-0002-0519-7717

apply at high speed, power and the installation environment is restricted. These problems of DC motors have been greatly improved by the use of AC motors.In particular, among the various types of AC motors, induction motors have a nonlinear multi-variable control structure, and thus they are mainly used for constant speed applications because of the complicated speed control. However, with the development of control device, current control technology, power semiconductor technology and control theory, induction motors have characteristics similar to the performance of DC motors in the driving field that requires high performance and are relatively inexpensive and robust compared to DC motors and widely used in various power applications.

In addition, the induction motor is simple in structure and inexpensive and can overcome the structural problems of the DC motor, and with the introduction of the improved control method, it can obtain operation characteristics corresponding to the response characteristics of the DC motor and it's application is gradually expanding to such servo systems and machine tool drives which is essentially require fast acceleration and deceleration and high speed operation. In particular, with the application of the vector control and the direct torque control method to the field where instantaneous torque control or speed control is required, the area of the induction motor is being expanded by using a high speed large current switching element and a high performance processor(Kim et al., 2011; Yoon et al., 2009).

Direct vector control is a method of estimating magnetic flux by measuring magnetic flux using a sensor or stator voltage, current, etc. Indirect vector control calculates slip angular velocity from stator flux current and torque current, add rotor speed and uses that as the magnetic flux angle.

Direct torque control has the advantage of obtaining accuracy and quick response because it controls torque and magnetic flux independently. In addition, the control accuracy and switching frequency can be varied by adjusting the hysteresis band width of the controller inputting the error of the magnetic flux and the torque.

Vector control, also called field-oriented control(FOC), is a variable-frequency drive(VFD) control method in which the stator currents of a three-phase AC electric motor are identified as two orthogonal components that can be visualized with a vector. that is, a high transient response by separating flux current component having the same direction as the rotor magnetic flux vector and the perpendicular torque current component on the reference frame that the stator current vector rotates at the synchronous speed and controlling the magnetic flux and torque, respectively. For vector control of induction motor, the rotation angle of magnetic flux and the magnitude of magnetic flux must be obtained. According to the method of obtaining this value, it can be divided into direct vector control and indirect vector control.[WU, 2006]

In this paper, we proposed an indirect vector method of the hysteresis current control technique which has low ripple and excellent control performance in the low speed operation comparing with the conventional DTC(Direct Torque Control) method used in the large merchant ship. The speed and current response characteristics were confirmed by applying the step input load torque and speed command through the PSIM program, and the characteristics of the conventional DTC method and the vector control method proposed in this paper were compared and analyzed.

Ⅱ. Materials and Methods

1. Direct torque control[DTC]

The values that calculate torque and stator magnetic flux by measuring voltage and current in induction motor and compare torque and magnetic flux command every cycle and the errors of torque and magnetic flux determined by the control accuracy of torque and magnetic flux respectively are inputs to the Hysteresis controller. The output of the hysteresis controller is used as the input of the lookup table of the voltage vector, and the desired voltage vector is found here and out-putted.

Direct torque control controls torque and magnetic flux independently, so you can get fast response with accuracy.

The stator flux can be expressed by Eq.(1) by the voltage equation of the induction motor on the three-phase stationary coordinate system.

$$V = R\,I + p\,\lambda \quad \cdots\cdots (1)$$

The value of stator flux in Eq.(1) is obtained as Eq.(2).

$$\begin{aligned}\lambda_s &= \int (v_s - R_s i_s)\,dt \\ &= V_s \cdot t - R_s \int i_s\,dt \quad \cdots\cdots (2) \\ &= \frac{2}{3}E[S_a + S_b \exp(j\frac{2\pi}{3}) + S_c \exp(j\frac{4\pi}{3})] \cdot t \\ &\quad - R_s \int i_s\,dt + \lambda_s\,|_{t=0}\end{aligned}$$

Since the stator resistance is very small in Eq.(2), assuming that the voltage drop $R_s i_s$ is very small compared to the first term and neglected, the stator flux is proportional to the magnitude of the stator voltage and the direction can be thought of as the same vector.

The relationship is expressed by the Eq.(3).

$$\Delta\lambda_s \approx V_s\,\Delta t \quad \cdots\cdots (3)$$

Here, Δt is the sampling period.

That is, the magnetic flux of the stator moves in the same direction as the stator voltage vector $\overrightarrow{V_s}$. If $\overrightarrow{V_s}$ is an effective vector, λ_s moves at a constant rate with the output voltage vector of the inverter, and at a very small speed if it is an ineffective vector. Therefore, the rotational speed of the magnetic flux is controlled by the ratio of the effective and the ineffective vector of the inverter output voltage.

<Table 1> shows the voltage vectors selected when the stator flux is in the North area. nth region. The vector of the magnetic flux has the direction of selecting the magnetic flux and torque of the motor according to the eight voltage vectors that the inverter can output and the output voltage vector of the inverter selected at the current position. The switching vector is selected considering the direction as well as the magnitude of the magnetic flux.

<Table 1> Selected vector and means.

V(n)	Radial positive voltage vector
V(n+1)	Forward positive voltage vector
V(n+2)	Forward negative voltage vector
V(n+3)	Radial negative voltage vector
V(n-1)	Backward positive voltage vector
V(n-2)	Back ward negative voltage vector
V(0)	Zero voltage vector

[Fig. 1] shows the concept of direct torque control, showing the switching vector and the flux vector. The moving direction of the magnetic flux

rotated by the selection of the switching vector in the hysteresis band is shown. The magnetic flux rotates, creating the trajectory of a pulsating circle.

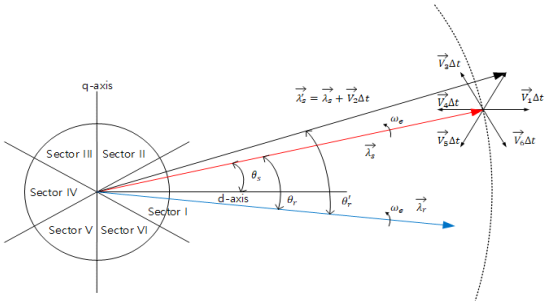

[Fig. 1] Conception of direct torque control.

Equation(4) relates to the hysteresis band of the magnetic flux.

$$(|\lambda_s|^* - \Delta|\lambda_s|/2) \le (|\lambda_s|) \le (|\lambda_s|^* + \Delta|\lambda_s|/2) \quad \cdots\cdots (4)$$

The choice of flux vector is also related to the magnitude and direction of rotation within the hysteresis width.

First, if the magnetic flux rotates in the clockwise direction, $\overrightarrow{V_6}$ is selected when the magnetic flux is in contact with the lower line of the hysteresis width, and $\overrightarrow{V_5}$ is selected when the magnetic flux is in contact with the upper line of the hysteresis band.

If you are rotating counterclockwise, select $\overrightarrow{V_2}$ and $\overrightarrow{V_3}$. Once the magnetic flux is determined, the torque is determined by equation(5).

$$T_e = \frac{3P}{2}\frac{L_m}{\sigma L_s L_r}\lambda_s \lambda_r \sin\theta_T \quad \cdots\cdots (5)$$

When the value of torque T_e reaches the torque command value T_e^*, T_e is preferably reduced as late as possible to reduce the switching frequency of the inverter.

It is better to use the ineffective vector among the switching vectors of the inverter, and the torque is divided into two cases according to the rotation direction.

$T_e^* - \Delta T_e \le T_e \le T_e^*$ when λ_s rotates clockwise

$T_e^* \le T_e \le T_e^* + \Delta T_e$ when λ_s rotates counterclockwise

Assuming that λ_s rotates clockwise, an ineffective vector is selected to stop λ_s and reduce T_e when T_e reaches T_e^*.

On the contrary, when T_e approaches $T_e^* - \Delta T_e$, an effective vector is selected to rotate the magnetic flux clockwise.

To calculate the optimal voltage vector in the optimal switching voltage vector lookup table, we need to know the stator flux position. This position can be obtained from equations(6a), (6b) and (6c) from the α-axis and β-axis values of the stator linkage flux in the stationary reference frame.

$$\overrightarrow{\lambda_s} = \lambda_{\alpha s} + j\lambda_{\beta s} = \int (v_{\alpha s} - R_s i_{\alpha s})dt + j\int (v_{\beta s} - R_s i_{\beta s})dt \quad \cdots\cdots (6a)$$

$$\lambda_s = \sqrt{\lambda_{\alpha s}^2 + \lambda_{\beta s}^2} \quad \cdots\cdots (6b)$$

$$\theta_s = \tan^{-1}\left(\frac{\lambda_{\beta s}}{\lambda_{\alpha s}}\right) \quad \cdots\cdots (6c)$$

Here $v_{\alpha s}$, $v_{\beta s}$, $i_{\alpha s}$, $i_{\beta s}$ are the measured stator currents and voltages.

Therefore, the torque is as shown in equation(7).

$$T_e = \frac{3}{2}\frac{P}{2}(i_{\beta s}\lambda_{\alpha s} - i_{\alpha s}\lambda_{\beta s}) \quad \cdots\cdots (7)$$

[Fig. 2(a)] shows the flux hysteresis controller. Since the stator flux always has a (+) value, the comparator output consists of two stages (1, 0). That is, $\Delta\lambda_s$ = 1 when the stator flux error is larger than the positive hysteresis width H_F , and $\Delta\lambda_s$ = 0 when it is smaller than the negative hysteresis width $-H_F$.

[Fig. 2(b)] shows the torque component hysteresis comparator used in the direct torque control inverter. In general, unlike the magnetic flux component hysteresis comparator, the output ΔT_e is thre e steps (-1.0.1) so that the torque command in both the forward and the reverse direction can be followed.

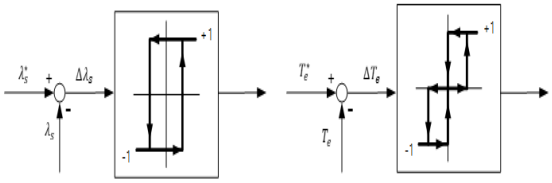

[Fig. 2] Characteristics of torque and flux hysteresis comparator.

<Table 2> Optimum switching voltage vector look-up table

Comparator Output		Sector					
X_λ	X_T	I	II	III	IV	V	VI
+1	+1	$\overrightarrow{V_2}$	$\overrightarrow{V_3}$	$\overrightarrow{V_4}$	$\overrightarrow{V_5}$	$\overrightarrow{V_6}$	$\overrightarrow{V_1}$
+1	0	$\overrightarrow{V_0}$	$\overrightarrow{V_0}$	$\overrightarrow{V_0}$	$\overrightarrow{V_0}$	$\overrightarrow{V_0}$	$\overrightarrow{V_0}$
+1	-1	$\overrightarrow{V_6}$	$\overrightarrow{V_1}$	$\overrightarrow{V_2}$	$\overrightarrow{V_3}$	$\overrightarrow{V_4}$	$\overrightarrow{V_5}$
-1	+1	$\overrightarrow{V_3}$	$\overrightarrow{V_4}$	$\overrightarrow{V_5}$	$\overrightarrow{V_6}$	$\overrightarrow{V_1}$	$\overrightarrow{V_2}$
-1	0	$\overrightarrow{V_0}$	$\overrightarrow{V_0}$	$\overrightarrow{V_0}$	$\overrightarrow{V_0}$	$\overrightarrow{V_0}$	$\overrightarrow{V_0}$
-1	-1	$\overrightarrow{V_5}$	$\overrightarrow{V_6}$	$\overrightarrow{V_1}$	$\overrightarrow{V_2}$	$\overrightarrow{V_3}$	$\overrightarrow{V_4}$

<Table 2> shows the optimal switching voltage vector lookup table based on the hysteresis comparator characteristics of torque and magnetic flux.

2. Direct Vector Control

This method, called magnetic flux feedback control, directly detects the air gap magnetic flux close a feedback loop on this signal by a Hall sensor or a sensing coil, or uses a magnetic flux model composed of motor terminal voltage, current and speed after that, magnitude and position of the rotor magnetic flux vector is obtained. In the direct measurement method, it is difficult to install mechanically because the Hall element or the detection coil must be installed in the stator slot, and the design of the filter is complicated because the harmonics generated by the slot vary with the motor speed. Therefore, it is common to use the magnetic flux vector estimated indirectly from the motor constant, voltage, current, speed, and the like.

2.1 Voltage Model of Stator Circuit

First, stator magnetic flux is obtained by integrating the stator voltage as shown in equations(8a) and (8b).

$$\lambda_{\alpha s} = \int (v_{\alpha s} - R_s i_{\alpha s})dt \quad \cdots\cdots (8a)$$

$$\lambda_{\beta s} = \int (v_{\beta s} - R_s i_{\beta s})dt \quad \cdots\cdots (8b)$$

Considering the influence of stator leakage flux, the rotor flux is calculated by the following equation.

$$\lambda_{\alpha r} = \frac{L_r}{L_m}(\lambda_{\alpha s} - \sigma L_s i_{\alpha s}) \quad \cdots\cdots (9a)$$

$$\lambda_{\beta r} = \frac{L_r}{L_m}(\lambda_{\beta s} - \sigma L_s i_{\beta s}) \quad \cdots\cdots (9b)$$

Here, $\sigma\ (= 1 - L_m^2 / L_s L_r)$ is the leakage

coefficient.

From the above equation, the rotor flux angle is obtained as follows.

$$\theta_e = \tan^{-1}(\frac{\lambda_{\beta r}}{\lambda_{\alpha r}}) \quad \cdots\cdots (10)$$

The above method is not accurate due to the influence of stator impedance drop and noise in the low speed region where the counter electromotive force is small, and the integrator is likely to be saturated due to the offset of the measurement variables during integration. Therefore, this method is mainly used in the high speed operation region by using a high pass filter instead of pure integration.

2.2 Current model of rotor circuit

In the low speed operation area, a method of calculating the magnetic flux from the rotor speed and the stator current is useful. In the case of a cage induction motor, since $v_{dr} = 0$ and the reference axis velocity $\omega_e = 0$ in the stationary reference frame and the d-axis and α-axis coincide, the following equation is obtained.

$$R_r i_{\alpha r} + \frac{d}{dt}\lambda_{\alpha r} + \omega_r \lambda_{\beta r} = 0 \quad \cdots\cdots (11)$$

The equation(12a) can be obtained by substituting in equation(11) by obtaining $i_{\alpha r}$ (in the stationary reference frame$i_{\alpha r} = i_{dr}$, $i_{\beta r} = i_{qr}$) from the linkage flux equation of the stator and rotor.

$$\frac{d\lambda_{\alpha r}}{dt} = \frac{L_m}{T_r} i_{\alpha s} - \omega_r \lambda_{\beta r} - \frac{1}{T_r}\lambda_{\alpha r} \quad \cdots\cdots (12a)$$

Here, $T_r (= \frac{L_r}{R_r})$ is the rotor time constant.

Similarly, the following equation is obtained from equations(11) and (12a).

$$\frac{d\lambda_{\beta r}}{dt} = \frac{L_m}{T_r} i_{\beta s} + \omega_r \lambda_{\alpha r} - \frac{1}{T_r}\lambda_{\beta r} \quad \cdots\cdots (12b)$$

The two equations(12a) and (12b) are calculated in real time by a microprocessor to estimate the magnetic flux. If these equations are expressed as vector differential equations, it becomes Eq.(13).

$$\frac{d\boldsymbol{\lambda}_r}{dt} = [-\frac{1}{T_r}\mathbf{I} + \omega_r \mathbf{J}]\boldsymbol{\lambda}_r + \frac{L_m}{T_r}\mathbf{i}_s \quad \cdots\cdots (13)$$

단, $\boldsymbol{\lambda}_r = [\lambda_{\alpha r} \quad \lambda_{\beta r}]$, $\boldsymbol{i}_s = [i_{\alpha s} \quad i_{\beta s}]$,

$$\mathbf{I} = \begin{bmatrix} 1 & 0 \\ 0 & 1 \end{bmatrix}, \quad \mathbf{J} = \begin{bmatrix} 0 & -1 \\ 1 & 0 \end{bmatrix}$$

The current model of the rotor circuit is suitable for estimating the magnetic flux in the low speed region. However, since the eigenvalue of equation (13) is $-1/T_r \pm j\omega_r$, the imaginary part becomes larger and oscillates easily when the speed increases. In addition, since the rotor resistance and the rotor inductance are used, when these motor constants are not accurate or when the motor constants change, the estimation value carries a large error.

3. Indirect Vector Control

This method, called slip frequency or feed-forward control, calculates slip command angular velocity using the magnetic flux current, torque current and motor constant on the synchronous rotational reference frame, and adds the rotor speed to the integral value, after that estimates and controls the field angle.

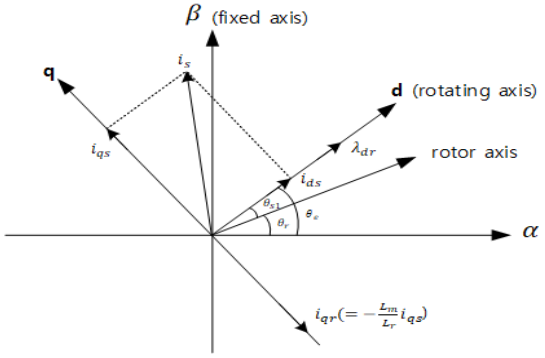

[Fig. 3] Vector diagram for indirect vector control.

It is a kind of predictive control. This method is sensitive to changes in motor parameters and requires encoders and resolvers for rotor speed information, but it is more widely applied because no flux sensor or model is required. To illustrate this control method, a vector diagram of the stator current vector decomposed into the current components of each reference axis is shown in [Fig. 3].

The $\alpha-\beta$ axis is fixed to the stator, the $d-q$ axis rotates at the synchronous angular velocity ω_e, and the rotor flux axis coinciding with the d axis rotates while maintaining a slip angle(θ_{sl}) with respect to the rotor axis(Refer to <Fig. 1>). Therefore, it can be seen that the magnetic flux current i_{ds} and the torque current i_{qs} of the stator separately control the rotor flux and the torque. In addition, the desired magnetic flux angle θ_e can be obtained by adding the rotational magnetic angle θ_r and θ_{sl} obtained from the magnetic flux setting value, it used for the coordinate transformation.

In the case of a squirrel cage induction motor, when the voltage equation of the rotor is converted into a synchronous rotational coordinate system, equations(14a) and (14b) are obtained.

$$\frac{d\lambda_{qr}}{dt}+R_r\, i_{qr}+\omega_{sl}\,\lambda_{dr}\;=\;0 \quad \cdots\cdots\cdots\cdots \text{(14a)}$$

$$\frac{d\lambda_{dr}}{dt}+R_r\, i_{dr}-\omega_{sl}\,\lambda_{qr}\;=\;0 \quad \cdots\cdots\cdots\cdots \text{(14b)}$$

Here, $\omega_{sl}\,(=\omega_e-\omega_r)$ is the slip angular velocity.

And, the $d-q$ axis rotor current component obtained from the stator and rotor linkage fluxes is expressed by equations(15a) and (15b).

$$i_{qr}\;=\;\frac{1}{L_r}(\lambda_{qr}-L_m\, i_{qs}\,) \quad \cdots\cdots\cdots\cdots \text{(15a)}$$

$$i_{dr}\;=\;\frac{1}{L_r}(\lambda_{dr}-L_m\, i_{ds}\,) \quad \cdots\cdots\cdots\cdots \text{(15b)}$$

Substituting equations(15a) and (15b) into equations(14a) and (14b) and eliminating the rotor current values results in equations(16a) and (16b).

$$\frac{d\lambda_{qr}}{dt}+\frac{R_r}{L_r}\lambda_{qr}-\frac{L_m}{L_r}R_r\, i_{qs}+\omega_{sl}\,\lambda_{dr}\;=\;0 \quad \cdots \text{(16a)}$$

$$\frac{d\lambda_{dr}}{dt}+\frac{R_r}{L_r}\lambda_{dr}-\frac{L_m}{L_r}R_r\, i_{ds}-\omega_{sl}\,\lambda_{qr}\;=\;0 \quad \cdots \text{(16b)}$$

When perfect vector control is performed in induction motor control, the q-axis component of the rotor linkage flux becomes zero and the d-axis component is also constant, so the torque is controlled only by the q-axis current component. Therefore, the following equation holds.

$$\lambda_{qr}\;=\;0 \quad \cdots\cdots\cdots\cdots \text{(17a)}$$

$$\frac{d\lambda_{qr}}{dt}\;=\;0 \quad \cdots\cdots\cdots\cdots \text{(17b)}$$

Substituting equation(17) into equations(16a) and (16b) yields equations(18) and (19).

$$\omega_{sl}\;=\;\frac{L_m}{T_r}\,\frac{i_{qs}}{\lambda_{dr}} \quad \cdots\cdots\cdots\cdots \text{(18)}$$

$$T_r \frac{d\lambda_{dr}}{dt} + \lambda_{dr} = L_m i_{ds} \quad \cdots\cdots (19)$$

In addition, in the case of constant flux control, $d\lambda_{dr}/dt = 0$, so that equation(20b) is obtained from equation(14b).

$$i_{qr} = -\frac{L_m}{L_r} i_{qs} \quad \cdots\cdots (20a)$$

$$i_{dr} = 0 \quad \cdots\cdots (20b)$$

Substituting the above equation into equations(18), (19) and (14), the following magnetic flux, slip and torque equations can be obtained.

$$\lambda_{dr} = L_m i_{ds} \quad \cdots\cdots (21)$$

$$\omega_{sl} = \frac{1}{T_r} \frac{i_{qs}}{i_{ds}} \quad \cdots\cdots (22)$$

$$T_e = \frac{3}{2} \frac{P}{2} \frac{L_m}{L_r} \lambda_{dr} i_{qs} \quad \cdots\cdots (23)$$

Therefore, Eqs.(20) to (23) are the motor models when the indirect vector control theory is applied to the induction motor and the magnetic flux angle is the following equation which is an integral value obtained by adding the motor angular velocity and the slip command angular velocity of Equation(23).

$$\theta_e = \int \omega_e \, dt = \int (\omega_r + \omega_{sl}) dt \quad \cdots\cdots (24)$$

So far, important vector control relations such as equations(20) to (23) have been derived from the rotor voltage and the rotor linkage flux equation of the vector control of induction motors. But, the stator voltage equation of the vector control induction motor must be known to construct a current controller that determines the performance of the actual vector control system.

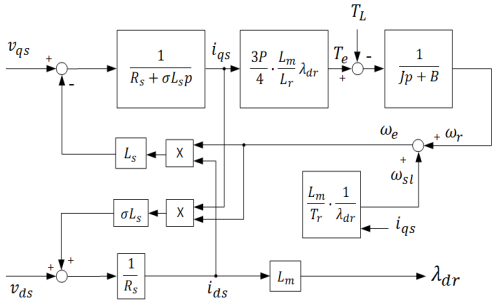

[Fig. 4] The block diagram of indirect vector controlled induction motor

This can be obtained by substituting the vector control relation equations (20a) and (20b) into the stator voltage equation and stator linkage flux equation, and the result is as follows.

$$v_{qs} = R_s i_{qs} + \sigma L_s p i_{qs} + \omega_e L_s i_{ds} \quad \cdots\cdots (25a)$$

$$v_{ds} = R_s i_{ds} - \omega_e \sigma L_s i_{qs} \quad \cdots\cdots (25b)$$

[Fig. 4] shows the induction motor model applying the indirect vector control theory based on the above results.

4. Induction Motor Control Using AFE Rectifier

4.1 AFE Rectifier

In small coastal ships such as cruise ships and small working ships, it is difficult to install a DFE rectifier that requires the installation of passive filters and phase shifting transformers to alleviate harmonics due to space constraints. Therefore, AFE rectifier, which is a kind of active filter, can be applied as a good technology(Jeon et al., 2017).

[Fig. 5] shows the AFE rectifier consisting of rectifier stage by connecting diode and IGBT in anti-parallel.

Each IGBT element in the rectifier stage is switched via PWM control. In the DC stage, a

small capacitor of 1/50 size was installed in place of the large capacitor, which is a disadvantage of the DFE method.(Hur et al., 2018).

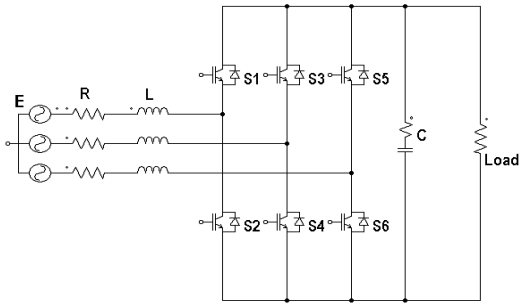

[Fig. 5] Circuit diagram of AFE rectifier.

4.2 Induction Motor Inverter

[Fig. 6] shows a typical induction motor speed control topology. Each IGBT element in the inverter stage is switched by PWM using the hysteresis current control equally for three speed control methods.

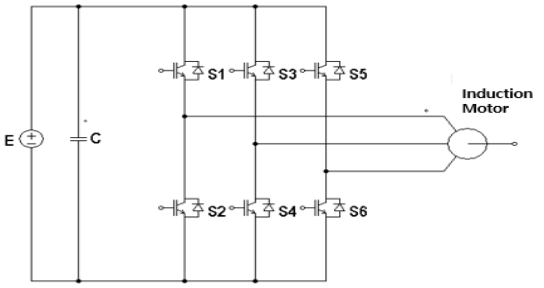

[Fig. 6] Circuit diagram of conventional converter.

Ⅲ. Results and Discussion

1. Simulation

In this paper, computer simulation is performed using PSIM program in high speed and low speed to verify the characteristics of three speed control methods of induction motor using AFE rectifier. Each speed control method is compared by switching to 100 [μs], which is the same as the inverter applied to small ships.

<Table 3> Parameters of induction motor and system constants used for computer simulation.

Rated output	3[HP]	R_r	1.56[Ω]
Rated voltage	220[V]	L_s	180[mH]
Rated current	9[A]	L_r	180[mH]
Rated speed	1735[rpm]	L_m	176[mH]
Poles	4	J (Moment of inertia)	0.1[Kg·m2]
R_s	2.0[Ω]	Sampling cycle	100[μs]

In the low speed region 300[rpm], step load torque was applied, and in the high speed region 1500[rpm], the load was proportional to the speed square. <Table 3> shows the parameters and system constants of the induction motor used in the simulation.

[Fig. 7] shows the PSIM block diagram of the induction motor drive simulation. Hysteresis controller is used to control current.

2. Induction Motor Simulation with Direct Torque Control

[Fig. 8] shows the speed response characteristics of the induction motor when the speed command is applied from 0[rpm] to 1,500[rpm]. (a) shows the change of motor speed and fine oscillation occurs compared to the vector control method. (b) shows the load change proportional to the speed square, and is similar to the conventional method in the transient state. (c) shows the phase current of the input stage and shows the sine wave similar to the vector control method.

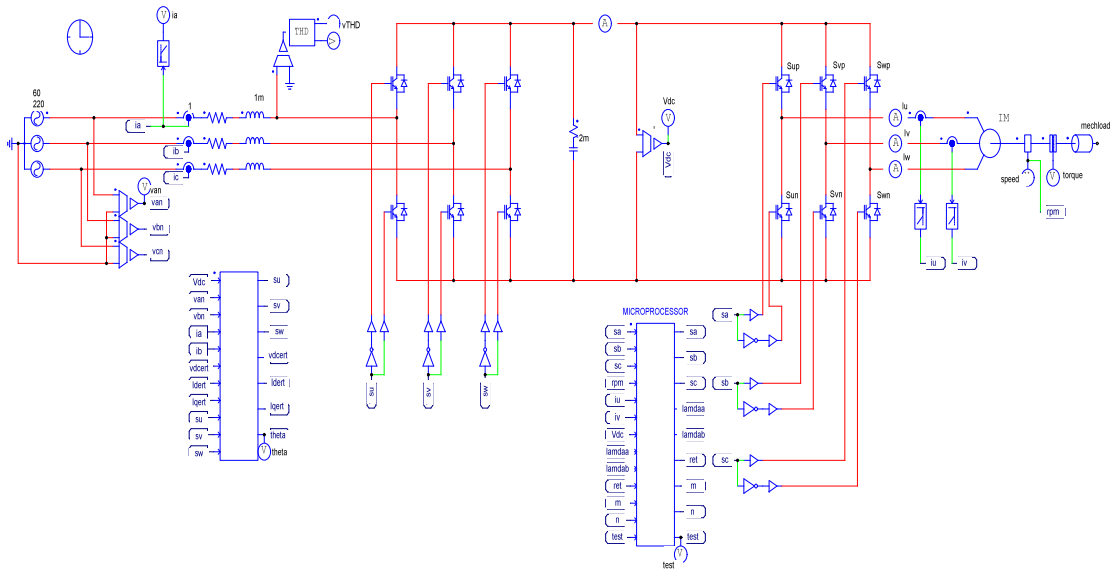

[Fig. 7] PSIM diagram of converter system.

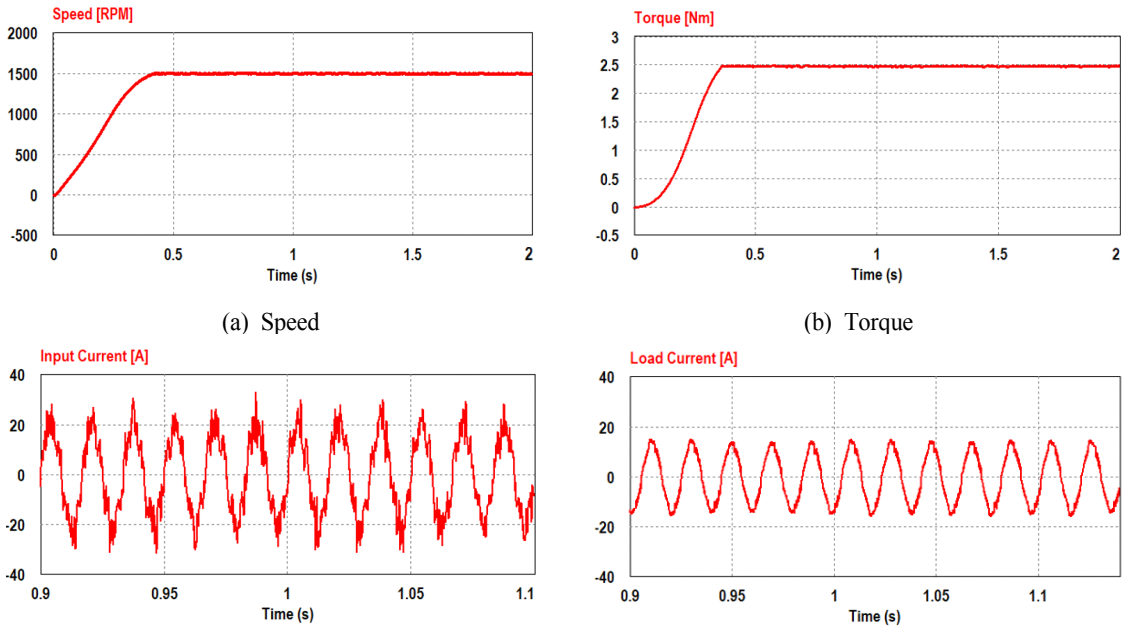

(a) Speed

(b) Torque

(c) Input current

(d) Load current

[Fig. 8] Simulation responses for step change of speed setting (0→1,500[rpm]).

THD is 6.59[%] and slightly higher than vector control. (d) is the motor maximum load current, and the maximum value is shown around 19[A] under the steady state.

[Fig. 9] shows the response characteristics of induction motor when load torque of 20[N·m] is applied during steady state operation at 300[rpm]. (a) shows the change of motor speed and oscillation is bigger than at high speed.

(b) shows the torque change before and after applying the load torque. (c) shows the change of shape of input phase current before and after load torque application, and the shape of input stage current is similar to the vector control method after load is stabilized. In addition, the change in current size due to the application of load torque is smaller than the conventional method. (d) shows the motor load current before and after applying the load torque, and after the load is stabilized, the maximum value flows around 24[A].

3. Induction Motor Simulation with Direct Vector Control

[Fig. 10] shows the speed response characteristics of the induction motor when the speed command is applied from 0[rpm] to 1,500[rpm]. (a) shows a change in motor speed, and (b) shows a load change proportional to the speed square.

(c) is a phase current waveform of the input terminal. THD contains 5.14[%], indicating that a good quality current is supplied. (d) shows the motor-side load current, and the maximum current is shown around 19[A] under the steady state.

[Fig. 11] shows the response characteristics when load torque of 20[N·m] is applied during steady state operation at 300[rpm] at one second after starting.

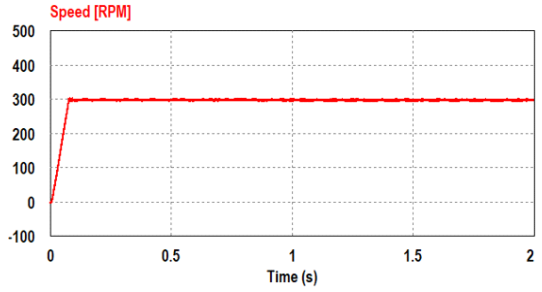

(a) Speed

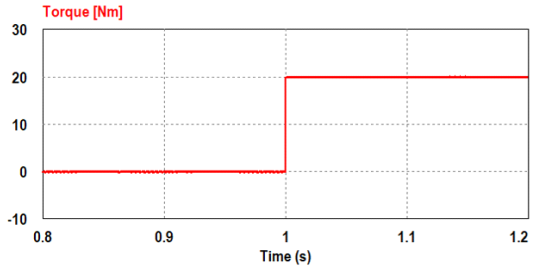

(b) Torque

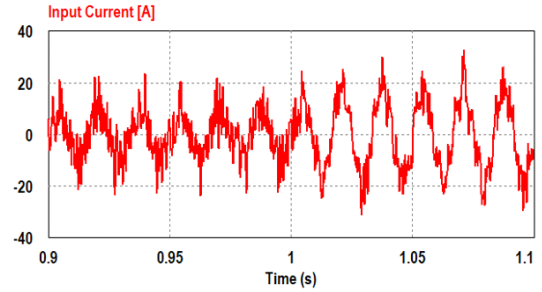

(c) Input current

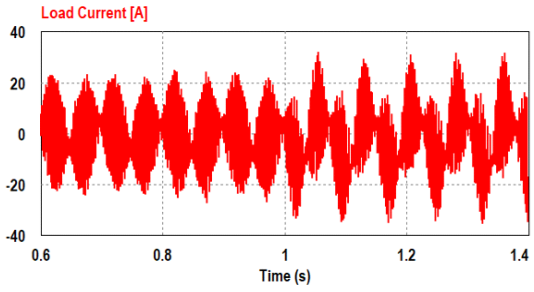

(d) Load current

[Fig. 9] Simulation responses for step change of load torque (300[rpm], 20[N·m]).

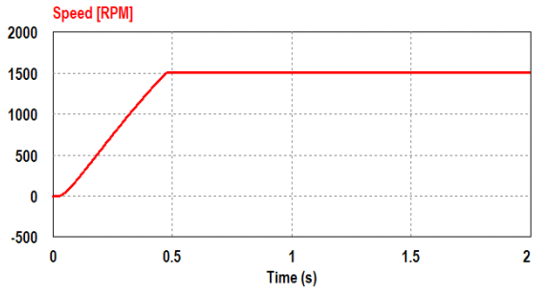

(a) Speed

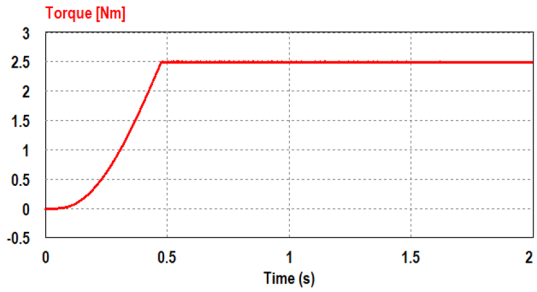

(b) Torque

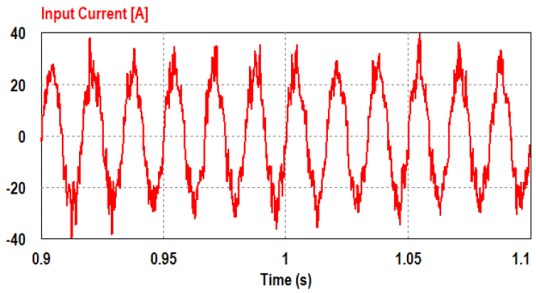

(c) Input current

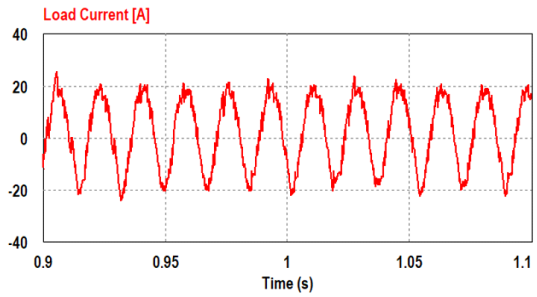

(d) Load current

[Fig. 10] Simulation responses for step change of speed setting (0→1,500[rpm]).

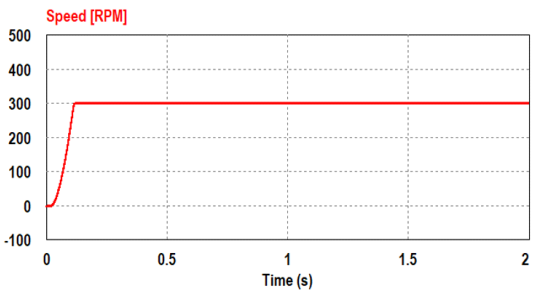

(a) Speed

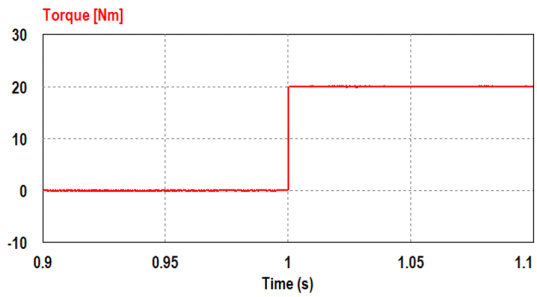

(b) Torque

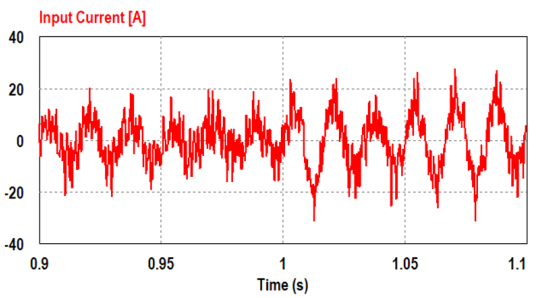

(c) Input current

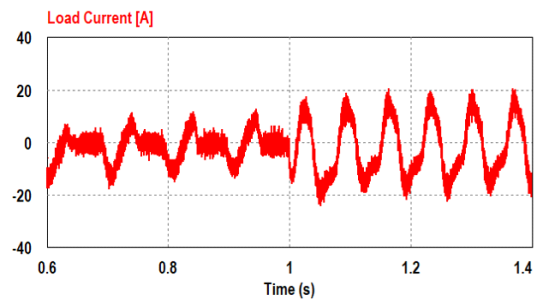

(d) Load current

[Fig. 11] Simulation responses for step change of load torque (300[rpm], 20[N·m]).

(a) shows the motor speed change, and (b) shows the torque change before and after applying the load torque. (c) shows the change of the phase current shape of the input stage before and after load torque application, (d) shows the motor load current before and after load torque application, and the maximum value is shown around 17[A] in the normal state.

4. Induction Motor Simulation with Indirect Vector Control

[Fig. 12] shows the speed response characteristics of the induction motor when the speed command is applied from 0[rpm] to 1,500[rpm]. (a) shows the change of motor speed and stable control result similar to the direct vector control method. (b) shows the load change proportional to the speed square and the wide load range similar to the direct vector control method in the transient state. (c) shows the input phase current and shows the same shape as the direct vector control method. The THD contains 4.97[%]. (d) shows the motor load current, and the maximum value is around 19[A] under the steady state.

[Fig. 13] shows the response when the load torque of 20[N ·m] is applied during steady state operation at 300[rpm].

(a) shows the motor speed change and stable control results under transient conditions similar to the direct vector control method. (b) shows the torque change before and after applying the load torque. (c) shows the change of shape of input

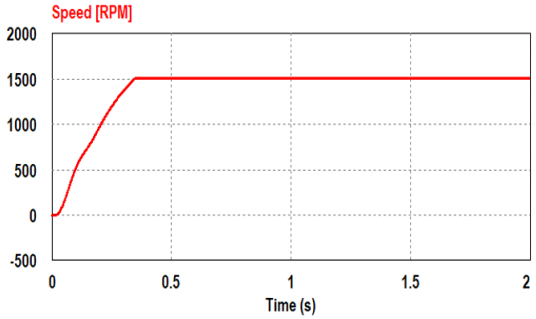

(a) Speed

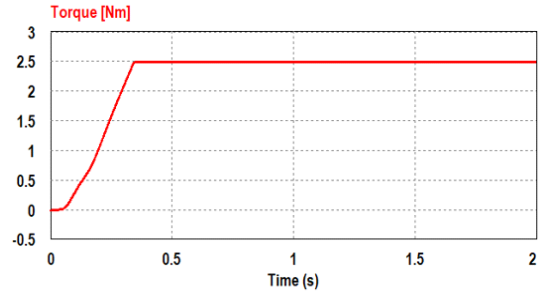

(b) Torque

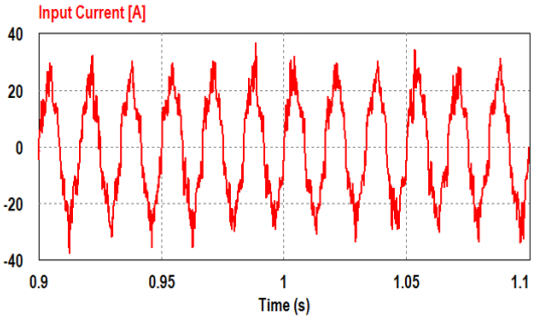

(c) Input current

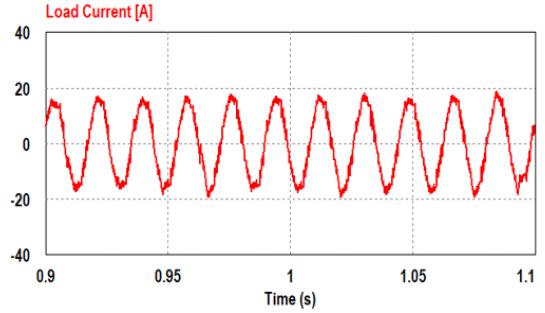

(d) Load current

[Fig. 12] Simulation responses for step change of speed setting (0→1,500[rpm]).

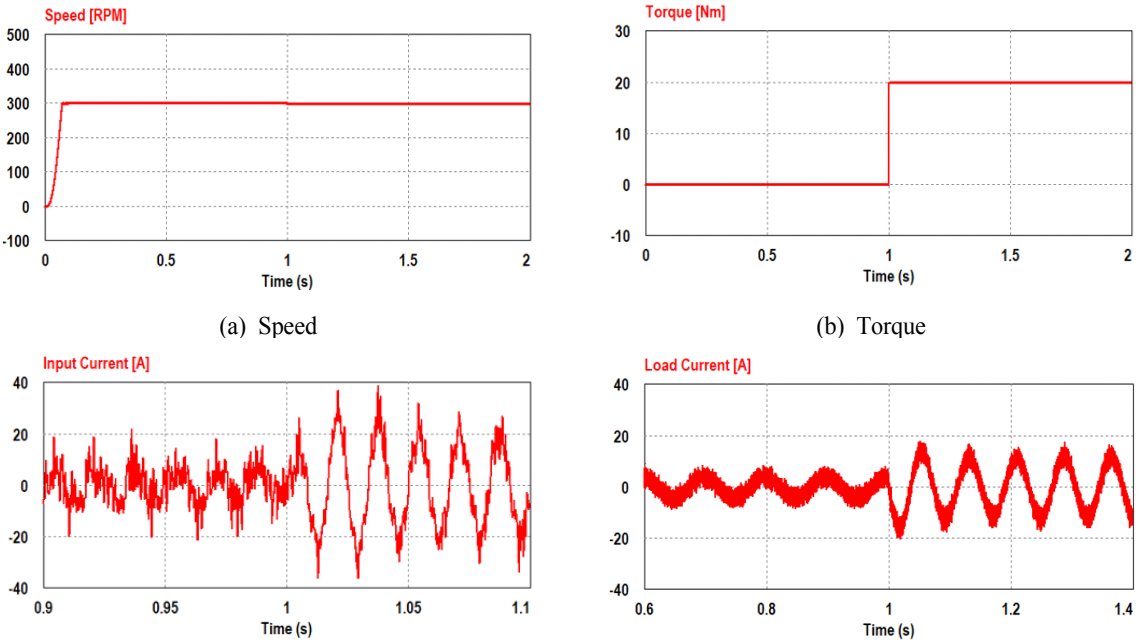

(a) Speed (b) Torque

(c) Input current (d) Load current

[Fig. 13] Simulation responses for step change of load torque (300[rpm], 20[N·m]).

phase current before and after applying load torque, and after the load is stabilized, the input current is closer to sine wave than direct vector control. In addition, the change of the current magnitude due to the load torque is larger than the direct vector control method. (d) shows the motor load current before and after applying the load torque, and the maximum value is about 17[A] after the load is stabilized. The results show the effectiveness of the control of system in a steady state as well as in transient stability.

5. Review simulation results

When comparing Fig. 8(a), Fig. 10(a), Fig. 12(a) and Fig. 8(b), Fig. 10(b), Fig. 12(b), respectively, speed command is applied from 0[rpm] to 1,500[rpm], which is a high speed range, it can be seen that stable control is achieved in the direct vector control and indirect vector control methods in the transient area. And in the direct torque control, fine oscillation occurs, but it is confirmed that it is relatively stable.

When comparing Fig. 8(c), Fig. 10(c) and Fig. 12(c), the THD of the direct torque control method is 6.59[%] and higher than THD of the direct vector control method 5.14[%], and the indirect vector control method THD 4.97[%] shows a current waveform close to the sine wave, indicating that the input current is very good quality.

When comparing Fig. 8(d), Fig. 10(d), and Fig. 12(d), the maximum value of the load current in the steady state section is not significantly different before and after 19[A] similarly, in the transient state, it was confirmed that the current is stably controlled in all three methods.

When comparing Fig. 9(a), Fig. 11(a), Fig. 13(a)

and Fig. 9(b), Fig. 11(b) and Fig. 13(b), the speed command is given from 0[rpm] to 300[rpm], the low speed range, the load is applied, it can be seen that fine oscillation occurs in the direct vector control method and continuous oscillation occurs in the direct torque control method as compared to the indirect vector control method which is stably controlled.

When comparing Fig. 9(c), Fig. 11(c), and Fig. 13(c), the waveform shows a near sine wave in the steady state section after the load is applied, indicating that the quality of the input current is excellent, and it is confirmed that the magnitude of the current change is large in the indirect vector control method.

When comparing Fig. 9(c), Fig. 11(c), and Fig. 13(c), after applying the load torque, it can be seen that the average values of the load current between the conventional method and the proposed method are about 17[A] in the steady state section, we can see that the difference is not big, and even during transient states, the proposed method is similar to the existing method and it was confirmed that stable control is possible.

As a result of comparing the switching frequency and gain value similar to the actual operation of electric propulsion system for small crafts, the indirect vector control method is superior in input current quality and speed control performance of induction motor for propulsion of small electric propulsion ship comparing with the direct torque control method used in large ships.

Ⅳ. Conclusion

Computer simulations using PSIM program were conducted for three control methods of propulsion induction motors equipped with AFE rectifiers applied to small craft. The results are as follows.

1. In the high speed range of 1,500[rpm], it is confirmed that the three control methods are relatively stable speed control under steady state.
2. The THD included in the input current is lower in the vector control method than in the direct torque control method.
3. It was confirmed that the speed and torque are controlled more stable in the vector control method than in the direct torque control method where oscillation occurs in the low speed range of 300[rpm].
4. In the case of a small propulsion motor, the indirect vector control method is expected to be the optimum if the same control method is applied in the high speed and low speed range.

References

BIN WU(2006), High-Power Converters and AC Drives, Wiley-interscience, 332~350

Haresh P and Ankit S(2016), A novel control method for UPS battery charging using Active front End(AFE) PWM rectifier., IEEE power electronics, Drives and Energy System, Trivandrum, India, December 14-17, 978~980. https://doi.org/10.1109/PEDES.2016 .7914232

Hur JJ, Kang KW, Kim JS and Kim SH(2018), Speed control for direct current motor using an AFE rectifier, Journal of the Korean Society of Marine Engineering, 42(10), 892~836. https://doi.org/10.5916/jkosme.2018 .42.10.829

Jeon JM, Kim SW and Kim JS(2018), A Study on Application of Electric Propulsion System using AFE Rectifier for Amall Coastal Vessles, Journal of the Korean Society of Marine Environment & Safety, 24(3), 373~380. https://doi.org/10.7837/kosomes.2018.24.3.373

Jeon HM, Yoon KK and Kim JS(2017), A study to Improve the DC output Waveforms of AFE Three-Phase PWM Rectifiers, Journal of the Korean Society of Marine Environment & Safety, 23(6), 739~745. https://doi.org /10.7837/kosomes.2017.23.6.739

Kim JS, Oh SG and Kim SH(2009), A Study on the Speed and Torque Control of Propulsion Motor for Electric Propulsion Ship by Direct Torque Contro, Journal of the Korean Society of Marine Engineering, 33(6), 946~951.

Kim JS, Oh SG, Kim SH, Kim HS, Kim DK and Yoon KK(2008), A Study on the Performance Analysis for Power Converters of Electric Propulsion Ship, Journal of the Korean Society of Marine Engineering, 32(8), 1278~1284.

Kim JS, Han WH and Seo DH(2012), Harmonic Reduction of Electric Propulsion System by Current Injection, Journal of the Korean Society of Marine Environment & Safety, 18(4), 360~364. http://dx.doi.org/10.7837/kosomes. 2012.18.4.360

Kim SY, Cho BG, and Sul SK(2013), Consideration of active ‐front-end rectifier for electric propulsion navy ship., IEEE Energy Conversion Congress and Exposition, Denver, USA CO, 13~19. https://doi.org/10.1109/ECCE.2013.6646675

Kim JS, Seo SD and Kim SH(2011), A Study on the Sensorless Speed Control of Induction Motor by New Direct Torque Control, Journal of the Korean Society of Marine Engineering, 35(8), 1105~1110, http://dx.doi.org/10.5916/jkosme. 2011.35.8.1105

Yoon KK, Oh SG, Kim JS, Kim YS, S. Lee SG and Kim SH(2009), A Study on the Sensorless Speed Control of Induction Motor using Direct Torque Control, Journal of the Korean Society of Marine Engineering, 33(8), 1261~1267.

• Received : 16 January, 2020
• Revised : 28 January, 2020
• Accepted : 06 February, 2020